Advances in Industrial and Manufacturing Engineering 10 (2025) 100158

Contents lists available at ScienceDirect

Advances in Industrial and Manufacturing Engineering

journal homepage: www.sciencedirect.com/journal/advances-in-industrial-and-manufacturing-engineering

3D-printed motorcycle seats: Replicating polymer foam performance for rapid prototyping and rider comfort

Andrea Montalti *, Patrich Ferretti, Fiammetta Spano, Alfredo Liverani

Department of Industrial Engineering, Alma Mater Studiorum University of Bologna, Bologna, Italy

ARTICLE INFO

Keywords:
Material extrusion (MEX)
Additive manufacturing
Stochastic infill
Rapid prototyping
Polymeric foams
Motorcycle saddle

ABSTRACT

The development of prototypes prior to the market launch of final products requires adapting production components to reduce costs and increase flexibility for potential modifications. While the manufacturing of rigid or structural components is well-established and widely practiced, the production of expanded materials presents significantly greater challenges due to the final product's reliance on the specific process employed. Changing the process to lower costs necessitates reproducing the same mechanical behaviour and appearance to ensure validation in terms of both style and function. This study focuses on replicating the behaviour of expanded polyurethane foam, commonly used in motorcycle seat padding, using thermoplastic polyurethane (TPU). The aim is to create a prototype or a customised version of the foam. The internal stochastic closed-cell structure is designed using slicing software, and test specimens are subsequently fabricated through Material Extrusion (MEX) additive manufacturing and subjected to compression testing. The results emphasise the critical influence of material hardness and infill density on the force-displacement curves. An experimental map, derived from three parameters (material hardness, elastic modulus, and foam density) illustrates the behaviour of the specimens, with iso-lines representing constant density. This map serves as a valuable tool for accurately replicating desired foam properties, providing guidance on material selection based on force-displacement characteristics.

1. Introduction

When the human body needs to interact with a rigid structure, polymer foams (Kabir et al., 2006) are one of the preferred materials. Application can be found for example in biomedical engineering (Alessandri et al., 2022), furniture, sports equipment, shoes, automotive and transportation (e.g., cars, buses, etc.), aeronautics, personal mobility (e.g., bicycles, motorbikes), as well as industrial equipment (Salifu et al., 2022) (e.g., agricultural, construction, forestry machinery, cranes, etc.). These foams (Liu et al., 2003), characterized by their internal structure of gas-filled cells (Chu et al., 2008), are employed in applications that require light weight, thermal insulation (Papadopoulos, 2005), and shock absorption. Motorcycle seats are predominantly made from polyurethane foams, owing to the numerous advantages they offer over other materials. These foams are durable and wear-resistant, providing comfort and support by conforming to the rider's body shape (Eida Nadirah et al., 2020). Their versatility allows them to be moulded into complex shapes, facilitating the mass production of seats that are both functional and aesthetically pleasing. Coatings and finishes can be applied to enhance resistance to moisture, UV rays, and other environmental factors, making these foams ideal for manufacturers due to their robustness and adaptability. In motorcycle racing, maintaining a stable and comfortable position is crucial for maximizing control and handling. Polymer foam seats offer excellent support, reducing the risk of fatigue during prolonged use. Additionally, they can be customised to fit the rider's body shape and size, ensuring a perfect fit for optimal performance. This customisation is essential in racing, where even minor differences in rider position can significantly impact performance.

One common traditional method for producing these foams is extrusion foaming, a technique that involves melting the polymer and then forcing it through a nozzle, resulting in an expanded structure (Pontiff, 2014). This process allows for relatively good control over the foam's density and cell size, although it has some limitations regarding the precision of cell morphology (Esposito et al., 2024). Another well-established methodology is mould foaming (Llewelyn et al., 2020) (Peng et al., 2024). This process is particularly valued for its ability to create foams with complex and precise shapes using preformed moulds

* Corresponding author
E-mail address: andrea.montalti8@unibo.it (A. Montalti).

https://doi.org/10.1016/j.aime.2025.100158
Received 13 August 2024; Received in revised form 18 February 2025; Accepted 19 February 2025
Available online 20 February 2025

(Feng et al., 2019). However, mould foaming is not without significant drawbacks, including the high costs associated with mould production and often lengthy lead times, which can limit its efficiency in large-scale production settings (Viscardi et al., 2016). A significant issue with extrusion foaming is the difficulty in achieving a well-defined cell morphology (Nian et al., 2024). The distribution and size of the cells can vary greatly depending on process parameters, directly impacting the material's mechanical and physical properties.

In response to these challenges, the scientific community has initiated numerous studies aimed at improving both the manufacturing techniques and properties of polymer foams. A notable innovation in this field is the use of thermally expandable microspheres (TEM) as blowing agents to create foams with controlled density (Pawar et al., 2022). TEMs, composed of a polymer shell encasing an expanding agent (Kalia et al., 2022), expand when heated, forming a cellular structure within the polymer matrix. Despite advances, precisely controlling cell morphology during 3D printing with TEMs remains a challenge. Simultaneously, the use of carbon dioxide (CO2) as a physical blowing agent in extrusion foaming (Zhou et al., 2023) has garnered attention for its environmental sustainability compared to traditional chemical agents. This technique, known as CO2 foaming, requires careful control of CO2 content and its diffusion during the 3D printing process to achieve uniform and stable foam structures.

Another emerging approach in foam (Ugadi et al., 2024) production leverages additive manufacturing technologies. These technologies enable the creation of flexible materials and geometric structures (Emery and Revier, 2022) designed to deform in a controlled manner in response to stresses or impacts. Although the literature on this methodology is still limited, some studies explore the development of custom filaments (Peng et al., 2021), from the base material such as TPU (Aghvami-Panah et al., 2024) to the production of filaments (Hassanien et al., 2023) for Material Extrusion (MEX) machines (Shin et al., 2022) (Kristiawan et al., 2021). Other documents suggest the possibility of obtaining foams through the use of co-extruded materials (WEN et al., 2017) or through multi-material printing, which allows for the creation of components with two or more integrated phases (H S et al., 2020). The adoption of additive manufacturing technologies for the production of polymer foams offers significant advantages over traditional methods. A critical aspect lies in the ability to customize the internal structure of the material, effectively eliminating defects caused by the uneven dispersion of the blowing agent. This precise control enables meticulous adjustment of both the external and internal geometry, including the infill configuration, thereby optimizing the mechanical properties of the 3D-printed component. The printing parameters play a significant role in determining the final properties of the component. To achieve high interlayer adhesion and minimize defects, the parameters were carefully defined based on insights from existing literature and experience with the specific machine and material used (Kechagias, 2024). Another advantage of this technology is the flexibility in producing small batches or prototypes. This capability eliminates the need for expensive moulds, significantly reducing initial costs and the time required to start production. 3D printing enables the rapid and efficient creation of functional prototypes (Parry et al., 2023), facilitating continuous iteration and innovation without the burden of traditional tooling.

The present study focuses on analysing the compression characteristics of samples created with a specific stochastic infill, which mimics the complex geometry of conventional foams. Stochastic structures are characterized by random geometries and shapes, distinguishing them from structures derived through topological optimization, as they are not generated based on the stress distribution within the material (Chisena and Shih, 2019), (Yi et al., 2023). The component can be analysed through simulation to evaluate its behaviour prior to fabrication (Yi et al., 2023). In this study, the stochastic infill was generated within the slicer to optimize the print head paths, thereby improving the manufacturing process. By examining these samples, the study aims to identify key parameters that influence the material's mechanical behaviour. This approach enables the correlation between infill, material hardness, and elastic modulus to be identified, using stochastic infill to emulate the behaviour of foams and optimize the performance of new samples.

Table 1
Filaments used and their intrinsic key characteristics.

	Hardness (Shore A)	Hardness (Shore D)	Density [g/cm^3]	Elongation at break [%]
Treed Elasto A	95	35	1.12	>200
Ninjatek Cheetah	95	35	1.22	580
Recreus Filaflex	82	31	1.12	650
Fiberlogy Fiberflex	81	30	1.07	870
Recreus Filaflex	70	20	1.08	900

2. Materials and methods

2.1. Filaments

To achieve characteristics equivalent to those of motorcycle polymer foam, research was undertaken to identify filaments that, once printed using material extrusion additive manufacturing, would exhibit similar behaviour. The study also examined internal geometry and printing parameters (Doshi et al., 2021). The focus was placed on various types of thermoplastic polyurethane (TPU) (Rodríguez-Parada et al., 2021), which can be processed in a molten state and is renowned for its versatility. TPU's unique structure provides excellent impact resistance, flexibility (Beloshenko et al., 2021), and a wide range of hardness levels, making it suitable for a variety of applications by mimicking rubber-like properties. These materials are hygroscopic (Seng et al., 2020), meaning they absorb moisture from the environment. If not properly dehumidified, this can lead to poor print quality due to bubble formation during the extrusion phase. Therefore, all materials used in the tests were dehumidified both before and during the printing process to ensure optimal results. Table 1 summarizes the material properties provided in the data sheets of the filament manufacturers. Only a selection of properties has been included, as the others were not always specified.

In addition to the material used to fabricate motorcycle foams, a key parameter for classifying commercially available foams is density. As previously mentioned, expanded polyurethane (Gama et al., 2018) is the most commonly used material for motorcycle seat production, and foams are categorized based on their density values. Therefore, it was necessary to conduct a benchmark analysis of the densities of foams used in this context to establish appropriate values for our project.

By consulting the catalogues of major suppliers of both foams and motorcycle seats, it was observed that the density of the products varies depending on the specific final application. Low-density foams are used in scooters and motorcycles designed for urban use to enhance comfort and assist the suspension in minimizing the transfer of loads to the rider. In contrast, off-road foams are typically harder, allowing the rider to slide on the seat, with comfort being a secondary consideration. For example, open-cell (Gong et al., 2005) expanded polyurethane has a density as low as 0.12 g/cm^3, while closed-cell (Chen et al., 2017) expanded polyurethane can reach densities as high as 0.4 g/cm^3. As a result, three representative density values were chosen: 0.12 g/cm^3, 0.21 g/cm^3, and 0.30 g/cm^3.

2.2. Slicer for 3D printing

As previously mentioned, MEX is a widely used 3D printing technology that utilizes a thermoplastic filament to construct physical

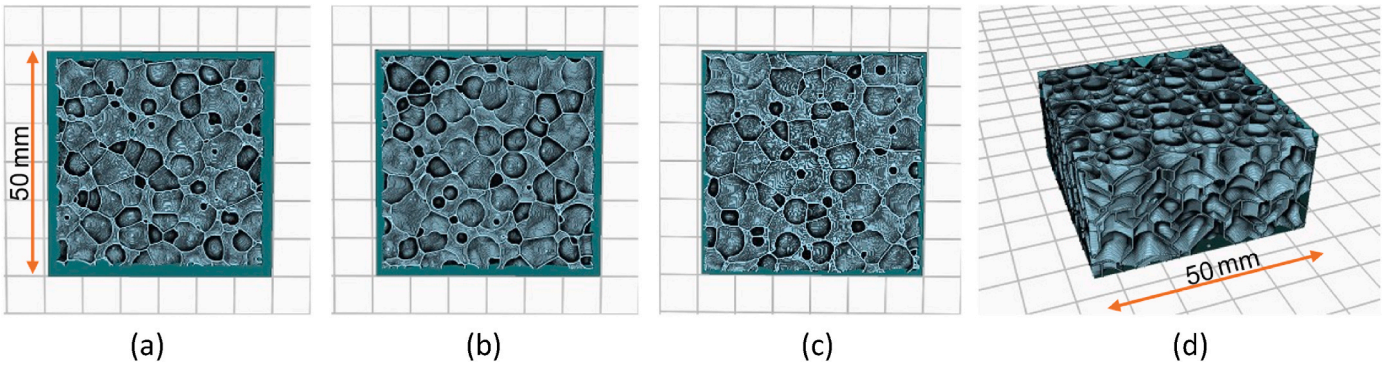

Fig. 1. Example of polyfoam infill: (a), (b), (c) section of the internal structure at different height, (d) prospective view.

objects layer by layer. The internal structure of the 3D printed object is defined by the infill (Forés-Garriga et al., 2020), which provides support and stability to the outer shell.

It allows for lightweighting components while maintaining high mechanical properties, forming a structure akin to a sandwich panel. This approach saves material and reduces printing times while still providing adequate support for the upper layers. There are two main categories of infill: planar and 3D. Planar infills are generated by extruding a 2D profile in the printing direction, while 3D infills lack a preferred direction as their structure develops in three dimensions. The mechanical behaviour of planar infill is predominantly unidirectional, maximizing mechanical properties in the printing direction. In contrast, 3D structures aim for more uniform behaviour in all three dimensions.

Various infill patterns are available, including linear, grid, triangular, honeycomb (Panda et al., 2018), and rectilinear for planar infills, and gyroid, cubic, and 3D triangular for 3D infills. The honeycomb pattern is one of the most commonly used for planar infill, known for its robust yet lightweight structure. Rectilinear infill is another popular choice, balancing strength and printing speed. Gyroid infill offers a mathematical pattern that provides a good compromise between rigidity and lightweight design. The selection of the appropriate infill pattern depends on the specific requirements of the printed object, including its size, shape, and intended application.

The goal was to identify an economical and easily replicable model that could effectively replicate the behaviour of motorcycle foams. The desired structure needed to exhibit similar behaviour in all three directions, with comparable mass and mechanical response to conventional foam. A model was selected that closely follows a stochastic pattern (Maiti et al., 2016), involving complex geometric structures (Bacciaglia et al., 2022) formed randomly and described as a collection of closed-cell bubbles. The cell shape was not perfectly spherical, as this would be inefficient to print, requiring supports and resulting in non-uniform wall thickness throughout the structure. Additionally, the required pattern must be easily crushable, allowing significant deformation under load without plastic deformation.

Among the available slicers (Anand Sankar et al., 2023), the IceSL slicer was ultimately chosen. In addition to the conventional infill patterns found in other software, this slicer provides a specific infill option called “polyfoam”. This infill pattern appeared to be the closest match to our project’s requirements, allowing us to achieve the desired internal structure (Fig. 1).

2.3. Choice of specimens

For the experimental specimens, the EN ISO 1923–1995 standard relating to cellular plastics and rubbers was followed. Once the methodology with which to generate the most suitable infill for production via MEX printing has been defined, a method must be found to obtain the desired density. Since the identification materials have different densities, to compensate for this difference, the infill of the specimens was adapted so as to have greater homogeneity in the results. The TPU filaments available on the market have a density that varies between 1.00 and 1.30 g/cm^3. By using a filament with a higher density than the material used for the production of the motorcycle foams, it is possible to print the specimens using an infill pattern such as is possible to play with the infill percentage to obtain a final result with a density close to the one obtained on conventional foams. Alternatively, by using a filament with a lower density compared to that used for the original sample, it is possible to increase the infill percentage to maintain the same density. However, it is important to consider that varying the infill can lead to changes in the mechanical properties of the sample, such as strength and rigidity. Therefore, considering the reference densities of the foams used in saddle production and the specific densities of the filaments used for printing, the infill values for all the specimens were determined. To obtain the percentages within Table 2, the proportion in Equation (1) was employed.

Table 2
Percentage of infill, with “Polyfoam" pattern, calculated using equation (1) considering the density of the chosen filaments.

Foam density target	0.12 g/cm^3	0.21 g/cm^3	0.30 g/cm^3
Treed Elasto A	10.71%	18.75%	(26.79%)
Ninjatek Cheetah	9.84%	17.21%	(24.59%)
Recreus Filaflex (82 A)	10.71%	18.75%	(26.79%)
Fiberlogy Fiberflex	(11.21%)	19.63%	28.04%
Recreus Filaflex (70 A)	(11.11%)	19.44%	27.78%

Note: Specimens obtained with the densities in brackets will not be subjected to compression testing because they do not exhibit characteristics similar to the reference foam through quality control.

$$\textit{infill density}\ \% = \frac{\textit{foam density target}}{\textit{filament density}} \bullet 100 \quad (1)$$

The cellular structure of foams enables the attainment of both low density and controlled energy absorption during deformation. Test specimens were printed to adhere to the standards specified in EN ISO 1923 for determining the force-displacement curve in compression for polymeric and flexible cellular materials. To comply with these standards, the test specimens were manufactured both by 3D printing and by cutting parallelepipeds with dimensions of 50 × 50 × 25 mm from commercial foam panels. This method ensures that the specimens align with the required standards and facilitates a consistent comparison between the 3D printed specimens and those derived from commercial foams.

2.4. Printing process

Printing parameters are essential for achieving high-quality results in Fused Filament Fabrication (FFF) 3D printing. Correctly configuring these parameters can significantly impact the accuracy and final

Table 3
Parameters used in the slicer for printing all specimens.

Parameter	Value	Unit of measure
First layer height	0.25	mm
Layer height	0.25	mm
Line width	0.4	mm
Print speed	30	mm/s
Retraction distance	0.5	mm
Retraction speed	40	mm/s
Support	No	/
Adhesion (Skirt/Brim/Raft)	Skirt	/
Cooling: fan speed	100	%
Enable Fan from layer	2	/
Solid layer: Top	3	/
Solid layer: Bottom	3	/
Number of shell	0	mm
Infill overhang angle	45	◦
Infill direction of anisotropy	0	◦
Minimum achievable percentage	Equal to infill percentage	%
Infill density	Equal to data in Table 1	%
Infill pattern	Polyfoam	/
Flow multiplier	Adjusted on demand	/
Nozzle temperature	220 ÷ 250	°C
Bed temperature	20 ÷ 60	°C

Table 4
Specimen weight and density recalculated considering the actual amount of material used. In mass value is reported the instrument accuracy.

	Low		Medium		High	
	Total mass[a] [g]	Real infill density [g/cm^3]	Total mass[a] [g]	Real infill density [g/cm^3]	Total mass[a] [g]	Real infill density [g/cm^3]
Reference foam	7.6	0.12	13.2	0.21	18.7	0.30
Treed Elasto A	10.2	0.11	16.8	0.22	22.5	0.31
Ninjatek Cheetah	10.7	0.11	16.9	0.21	22.8	0.31
Recreus Filaflex (82 A)	10.8	0.12	16.8	0.22	22.9	0.31
Fiberlogy Fiberflex	9.5	0.10	14.5	0.18	20.0	0.27
Recreus Filaflex (70 A)	9.7	0.10	15.2	0.19	20.0	0.27

[a] The accuracy of the instrument used is 0.1 g.

appearance of the printed object. Incorrect parameter settings can lead to issues such as deformation, filament extrusion problems, and poor adhesion between the various layers of the object. It is crucial to experiment with printing parameters to find the best combination for the type of filament used and the specific requirements of the object being printed, ensuring both high-quality printing and increased printing process reliability. For the selected filament type, the fundamental printing parameters were adhered to as specified in the datasheets, while some parameters were chosen to optimize specimen quality.

The aesthetic aspect plays a particularly influential role in the creation of functional prototypes, as it provides users with comprehensive feedback, enabling them to better identify potential modifications from both stylistic and functional perspectives. From a functional standpoint, it helps to detect defects that could alter the component's behaviour compared to its intended design. By examining the top and bottom layers, it is possible to assess the cohesion of the deposited lines within the same layer. To achieve this, the flow rate of the extruded material was adjusted. For the infill, proper deposition is essential, especially since flexible materials can face challenges during filament feeding through the extruder. The deposited lines must maintain consistency across all layers, avoiding a gradual reduction in flow as the layers build up, which could compromise adhesion between lines. Furthermore, correctly configuring retraction settings is vital to prevent stringing within the infill. Stringing could adversely affect the mechanical properties of the component, necessitating precise calibration to preserve both structural integrity and aesthetic quality.

For the production of the specimens, the Artillery Sidewinder X1 was employed. This printer, with its open-frame design and substantial print volume of 300 × 300 × 400 mm, is particularly well-suited for the fabrication of large objects. The extruder used was the LGX Shortcut Copperhead hot-end, a premium direct-drive hot-end for 3D printing. This component is distinguished by its minimal distance between the extruder motor and the nozzle (Xu et al., 2022). Such a configuration is particularly advantageous for flexible filaments, as it reduces the risk of buckling, which could otherwise compromise the print quality or cause clogging.

The test specimens were all produced using the same printing parameters, except for the nozzle temperature and bed temperature, which were adjusted according to the manufacturer's recommendations. These parameters are listed in Table 3.

Our objective is to produce a cube with three solid layers at both the top and bottom, ensuring a well-defined surface for both the printing and testing stages. Furthermore, when a point load is applied to the test specimen, multiple cells are engaged to facilitate better force distribution. External shells were excluded to assess the behaviour in a general context, avoiding the influence of shell lines which can alter stiffness. The overhang angle is fixed at 45° to eliminate the need for supports within the infill, thereby reducing printing errors. The infill's anisotropy

Fig. 2. Example of specimens (from left to right): Treed ElastoA (18,75%), Ninjatech Cheetah (24,59%), Filaflex Recreus 82 A (18,75%), Fiberology Fiberflex (28,03%).

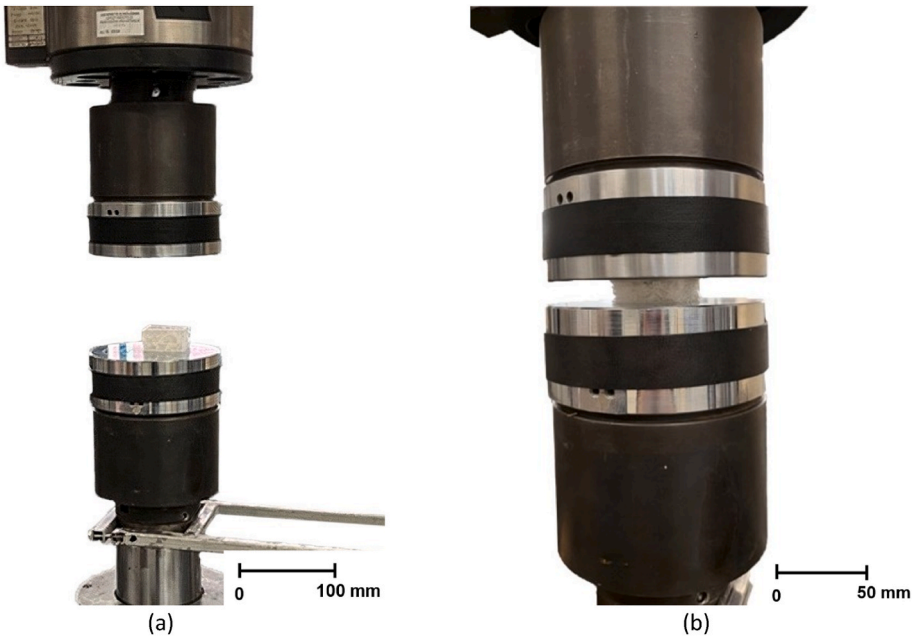

Fig. 3. Photo of the testing machine: (a) specimen in position; (b) compressed specimen.

direction is set to zero to create the most isotropic component possible. The infill density and the minimum achievable percentage vary for each test specimen, as previously specified. The initial flow multiplier is set to one and is adjusted based on the material used; it is modified if the flow during printing is insufficient or excessive, in order to improve the quality of the printed object.

Upon completion of the prints for creating the test specimens (Fig. 2), the material used was assessed using a digital scale to determine the actual density. Before calculating the actual density of the test specimen's infill, it is necessary to subtract the mass of the solid layers that were created (Table 4).

To conduct a focused evaluation, foams with properties and loads comparable to those typically employed in commercial applications were tested. Not all the specimens listed in Table 2 were subjected to compression testing, as a qualitative assessment revealed that some exhibited behaviour significantly different from that of the reference foam. Samples were compressed between two flat plates using an Instron 8032 universal testing machine equipped with a 25 kN load cell, as illustrated in Fig. 3. The crosshead speed was set at 5 mm/min, with a maximum displacement limit of 18 mm and a force limit of 5 kN.

The aim of the test is to describe the behaviour of the test specimens in order to characterize the material and the produced infill. The displacement was constrained to remain within the elastic range of the specimen, thereby preventing permanent deformation. After conducting tests on each of the previously mentioned test specimens, all data collected by the machine's operating software was filtered and reprocessed to facilitate comparisons and analyses.

3. Result

The data obtained from the compression tests were filtered and graphically represented to facilitate a series of comparisons. The trends

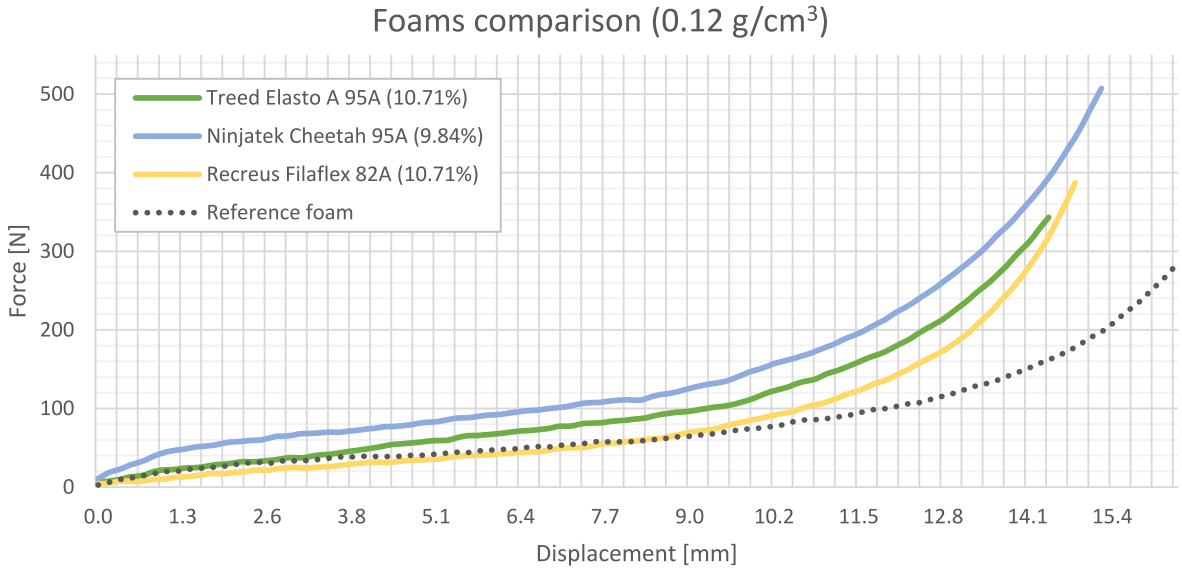

Fig. 4. Comparison between foams with a density 0.12 g/cm^3. Percentage in parenthesis indicates the Infill % for each material; all curves represented have a standard deviation of less than 7%.

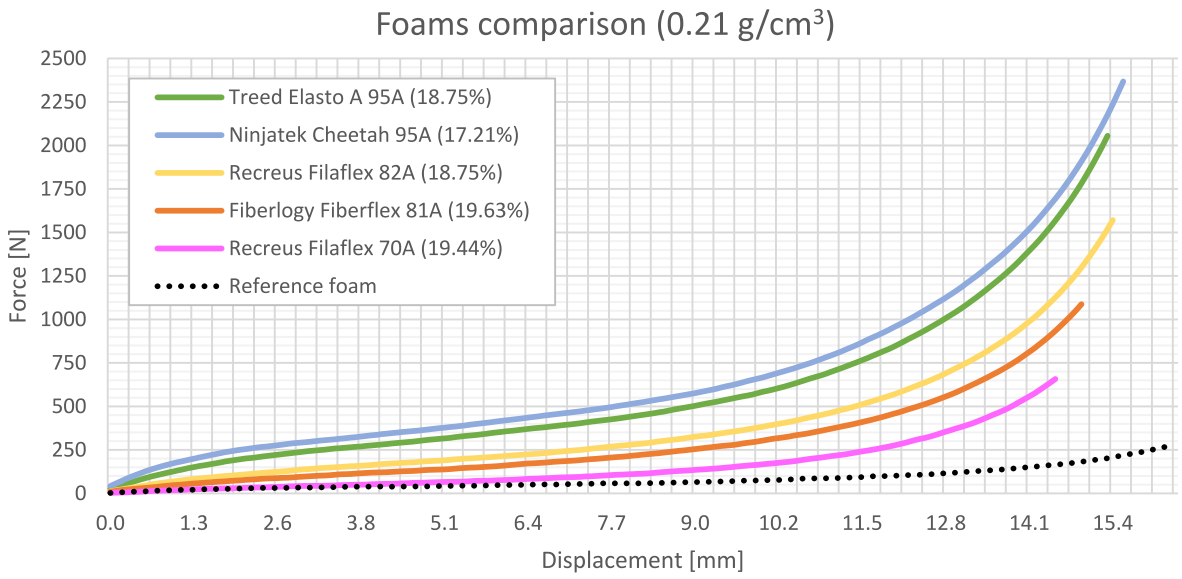

Fig. 5. Comparison between foams with a density of 0.21 g/cm^3. Percentage in parenthesis indicates the Infill % for each material; all curves represented have a standard deviation of less than 7%.

observed in the experimental graphs align with the theoretical behaviour of hyperelastic materials. Two distinct regions can be identified. In the initial region of the graph, where deformations are low, the behaviour is nearly linear, and the force increases proportionally with deformation, representing the elastic phase of the material. Beyond this, there is a non-linear region where the force increases non-proportionally with deformation, often displaying an “ascending" trend in the force - displacement curve. The graphs depicting these materials’ behaviour also include the zone of maximum deformation capacity, commonly referred to as the specimen’s rupture zone.

The tests conducted on these specimens do not exhibit rupture or plastic deformation because the intention was to remain within the elastic behaviour zone of the specimen. Upon initial analysis, it is evident that the specimens exhibit a similar trend to that of the reference foam, which was the primary objective of the research. Specifically, the reference foam has a density of 0.12 g/cm^3; thus, it can be compared to foams produced at the same density and subjected to compression testing.

As shown in Fig. 4, the reference foam initially displays a curve very similar to that of Treed Elasto A (Shore: 95 A), but in the central part of the graph, it more closely resembles the curve generated by Recreus Filaflex (Shore: 82 A). In the nonlinear final part of the graph, all specimens produced through additive manufacturing diverge from the behaviour of the reference foam, displaying a shorter linear zone and reaching a steeper slope with less deformation. This discrepancy is also due to the reference foam’s linear behaviour extending up to a displacement of 11.5 mm, whereas the 3D printed foams exhibit a linear zone up to approximately 9.0 mm of displacement.

It is noteworthy that Ninjatek Cheetah, despite having the same hardness as Treed Elasto A, behaves differently in the initial part of the graph and maintains this divergence throughout the remaining part of the graph. For displacements below 3.5 mm, the behaviour of the reference foam is better represented by the specimen made with Treed Elasto A. In contrast, for displacements between 3.5 mm and 9.0 mm, the

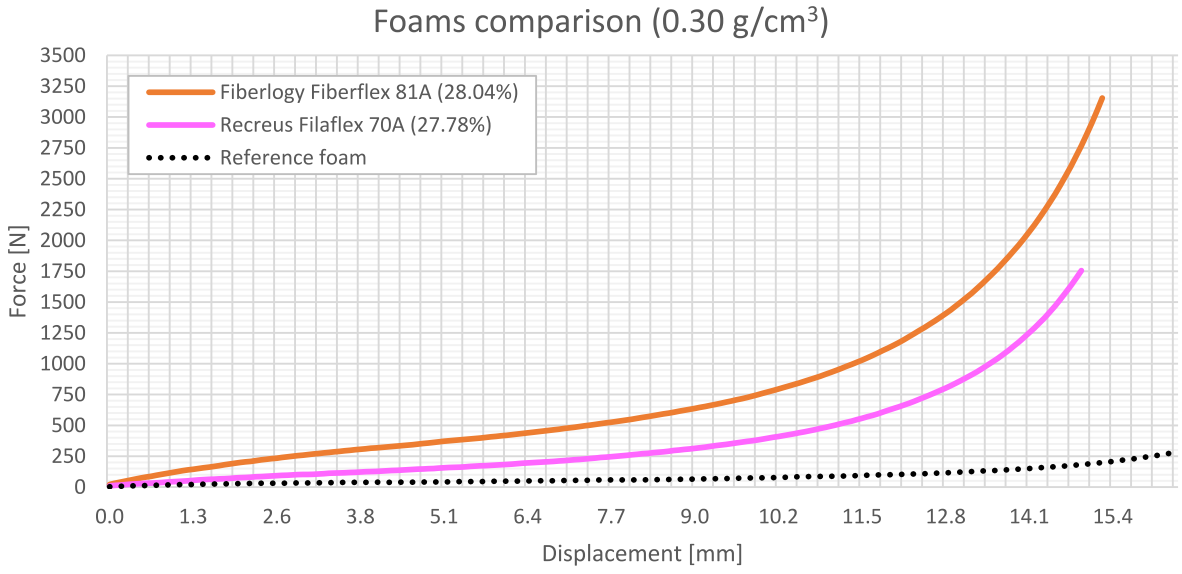

Fig. 6. Comparison between foams with a density of 0.30 g/cm^3. Percentage in parenthesis indicates the Infill % for each material; all curves represented have a standard deviation of less than 7%.

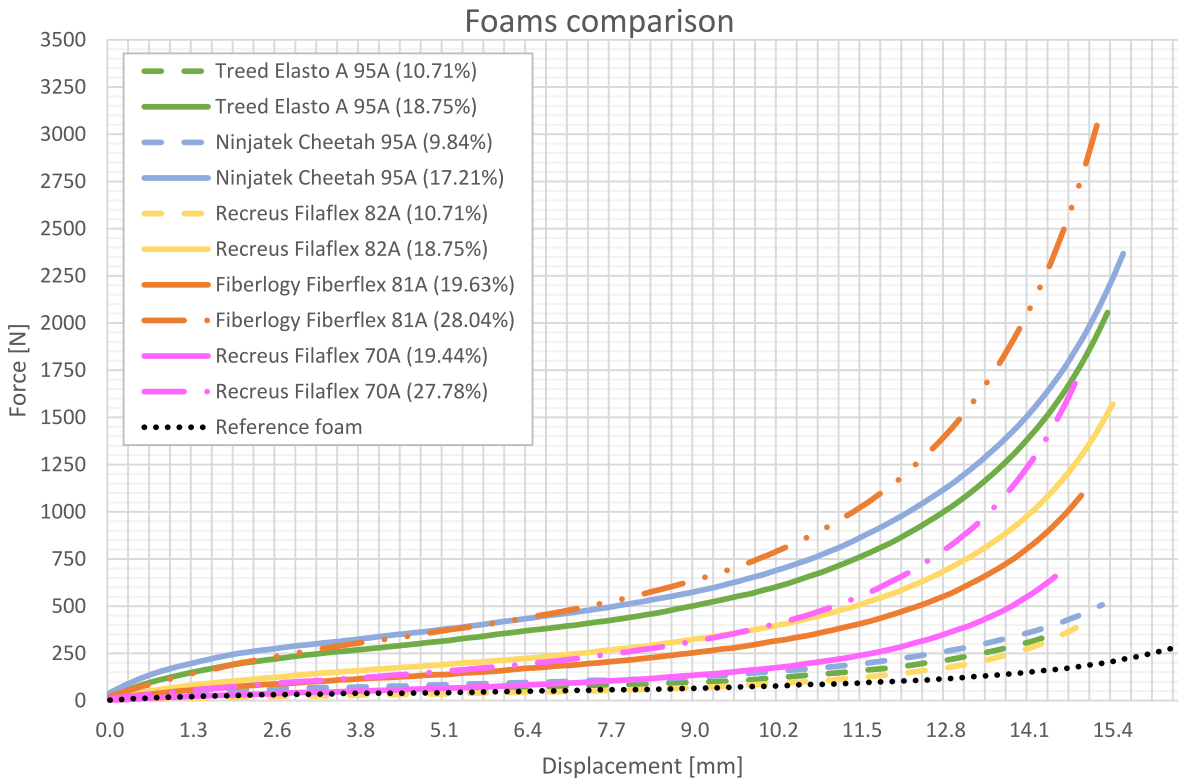

Fig. 7. Graph of all foams compared to the reference foam. Percentage in parenthesis indicates the Infill % for each material; all curves represented have a standard deviation of less than 7%.

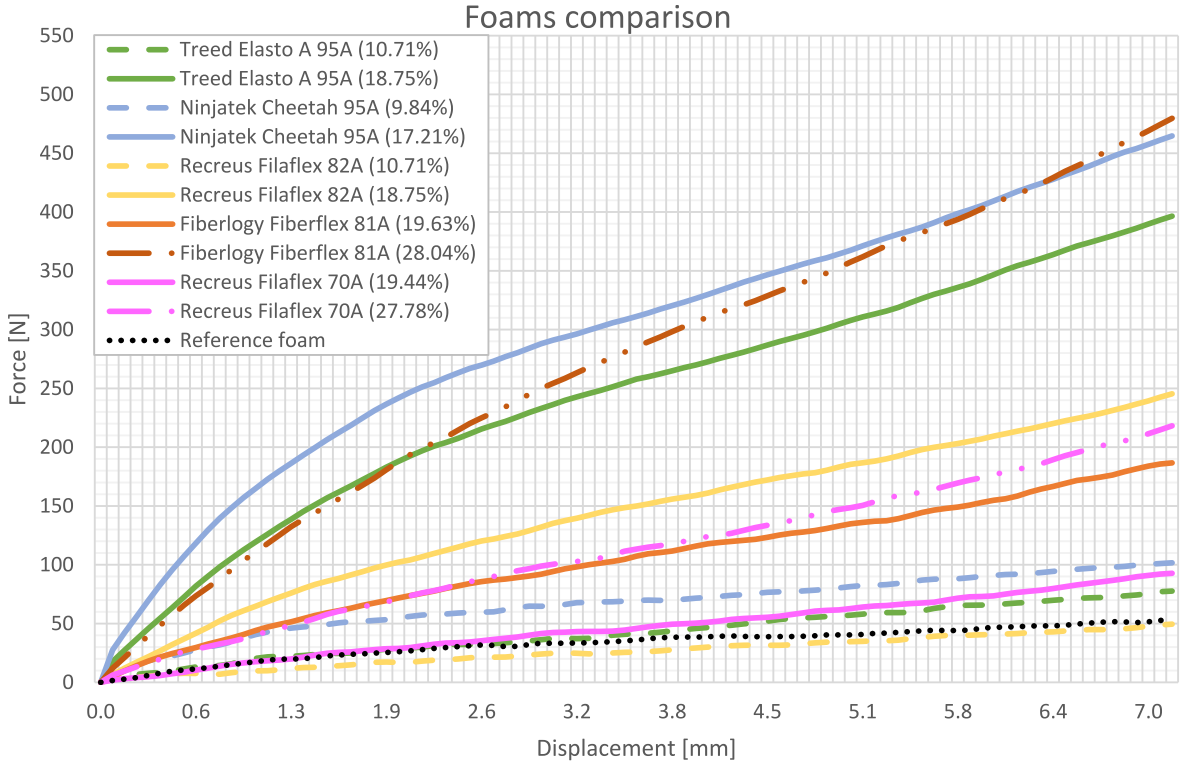

Fig. 8. Graph zoomed into the initial part of the deformation. Percentage in parenthesis indicates the Infill % for each material; all curves represented have a standard deviation of less than 7%.

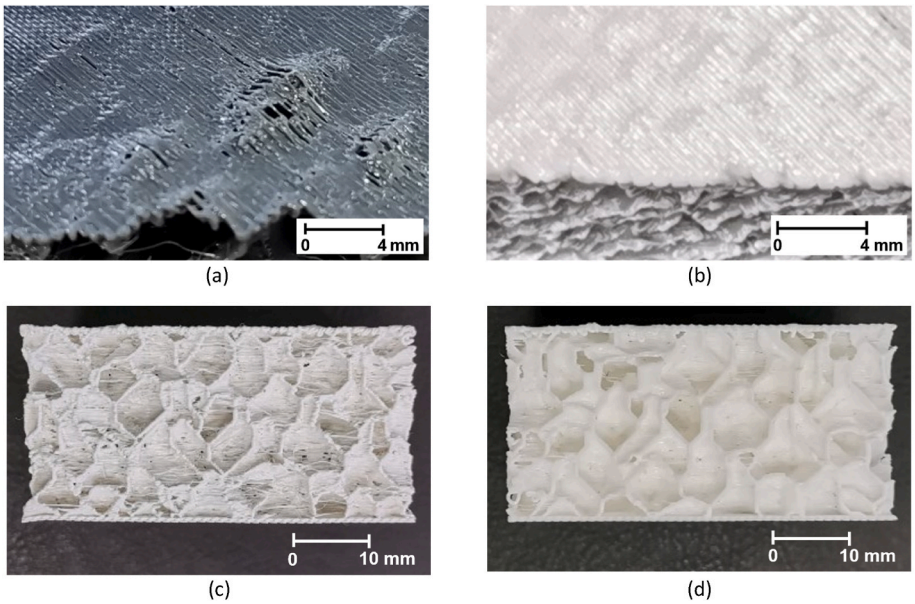

Fig. 9. Details of the printed specimens: (a) close-up of the top layer of a specimen exhibiting a fill defect; (b) close-up of the top layer of a correctly fabricated specimen; (c) infill showing significant material stringing; (d) infill correctly fabricated with minimal stringing.

behaviour of the reference foam is more accurately characterized by the specimen made with Recreus Filaflex 82 A.

Foams with a density of 0.21 g/cm^3 (Fig. 5) exhibit higher force values compared to those with lower densities observed earlier at the same displacement. The curves are ordered according to increasing filament stiffness, with the specimen made from Recreus Filaflex 70 A producing the lowest curve. As the material hardness increases, the force at the same displacement also increases.

Foams with a density of 0.30 g/cm^3 (Fig. 6) achieve even higher force values than those with lower densities. The linear behaviour zone is shorter, indicating that the nonlinear zone begins at a lower displacement. It is evident that specimens with higher densities exhibit greater reaction force compared to those with lower densities at the same displacement.

Figs. 7 and 8 present a comprehensive overview of all the tested specimens, providing a general perspective on the results.

Prior to testing, the specimens are meticulously inspected to detect any defects originating from the printing process, ensuring these do not affect the accuracy of the results. Fig. 9 provides an example of defects observed on the top layer, as well as significant stringing effects in the

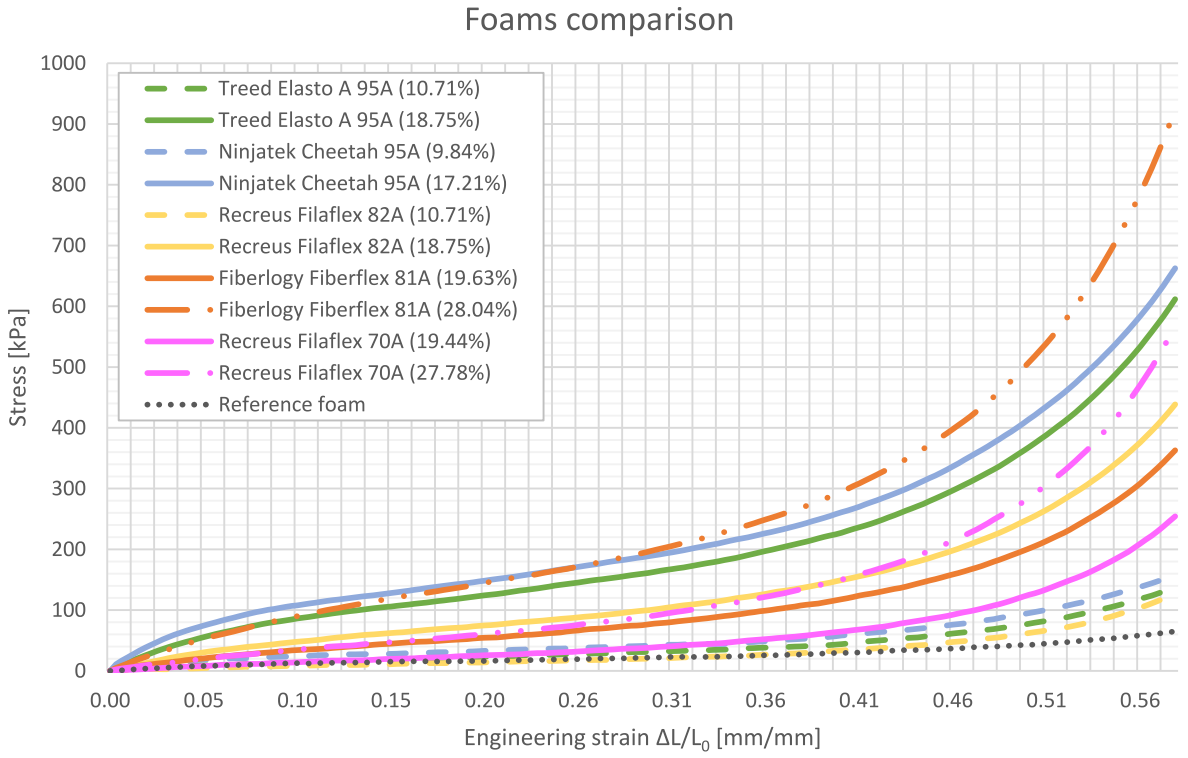

Fig. 10. Graph stress – engineering strain of all foams compared to the reference foam. Percentage in parenthesis indicates the Infill % for each material; all curves represented have a standard deviation of less than 7%.

Table 5
Slopes of the central linear area of the specimens.

	Infill %	Density [g/cm^3]	Shore (A)	Stress/strain [kPa]
Reference foam	/	0.12	/	46.93
Recreus Filaflex 82 A	10.71	0.12	82	62.40
Treed Elasto A	10.71	0.12	95	93.94
Ninjatek Cheetah	9.84	0.12	95	98.26
Recreus Filaflex 70 A	19.44	0.21	70	133.77
Fiberlogy Fiberflex	19.63	0.21	81	222.73
Recreus Filaflex 82 A	18.75	0.21	82	268.78
Recreus Filaflex 70 A	27.78	0.30	70	305.94
Treed Elasto A	18.75	0.21	95	397.79
Ninjatek Cheetah	17.21	0.21	95	432.05
Fiberlogy Fiberflex	28.04	0.30	81	543.30

infill region. Fig. 9 also highlights a structure with proper material deposition, free from any visible flaws. It is crucial to ensure that the specimens, both before and after the compression tests, do not exhibit permanent deformations or fractures that could irreversibly alter their characteristics. Standards specify a maximum allowable displacement during testing to prevent such occurrences. Moreover, this study aims to develop components capable of withstanding multiple compression cycles under normal usage conditions, without operating near the component's performance limits.

4. Discussion

Overall, the specimens exhibited the anticipated behaviour. The force-displacement (Fig. 8) curve features an initial non-linear region, which is more pronounced in some specimens than in others. This is followed by a linear region, the slope of which depends on the material and the infill. After the linear segment, there is another non-linear region with an increasing slope. Specifically, Fig. 7 provides an enlarged view of the initial section of the graph, enabling a detailed examination of the behaviour of specimens with reduced displacement. Within this region, substantial differences in the behaviour of the specimens are evident. Some, like Recreus Filaflex 82 A (10.71%), show a linear trend from the beginning, while others, such as Ninjatek Cheetah (17.21%), exhibit a pronounced initial nonlinear settling zone. Fig. 7 also illustrates how some specimens display a steep settling phase followed by a reduced slope in the linear zone compared to similar specimens. For instance, Fiberology Fiberflex (28.04%) starts with a reduced slope, lower than Treed Elasto A (18.75%) and Ninjatek Cheetah (17.21%) but surpasses their force values before reaching 7.0 mm of displacement due to a higher slope in the linear region.

Another example is Recreus Filaflex 70 A (27.78%), which behaves similarly to Fiberology Fiberflex (19.63%) up to a displacement of 2.1 mm. Beyond this point, it exhibits a higher slope, aligning its behaviour with Recreus Filaflex 82 A (18.75%) for deformations around 9.0 mm and even surpassing it in the nonlinear zone.

In both examples, a specimen made of a softer material shows an initial phase with a reduced slope compared to the other specimens but has a higher density. This results in a steeper curve slope in the central linear segment.

From the compression test behaviour of the specimens, the Stress-Engineering Strain curve can be calculated (as shown in Fig. 10) to understand the material's response under the applied load. Within the linear region of the curve in Fig. 10, the slope was determined as the ratio of stress to strain. This calculation allows for a comparison of the slopes across the various specimens, providing a means to evaluate their respective stiffnesses.

Table 5 lists the Stress/Strain values in ascending order, allowing for an analysis of how these values are influenced by the material's density and hardness. As the stress-strain ratio increases, a corresponding increase in density is observed, assuming the filament hardness remains constant. To better visualise the relationship between these parameters, a scatter plot has been employed, as shown in Fig. 11.

The graph in Fig. 11 characterises the behaviour of the specimens by correlating the elastic modulus, calculated as the ratio of stress to strain from the linear segments of the curves, with the bulk material hardness. The plot displays three distinct lines, each traversing clusters of points

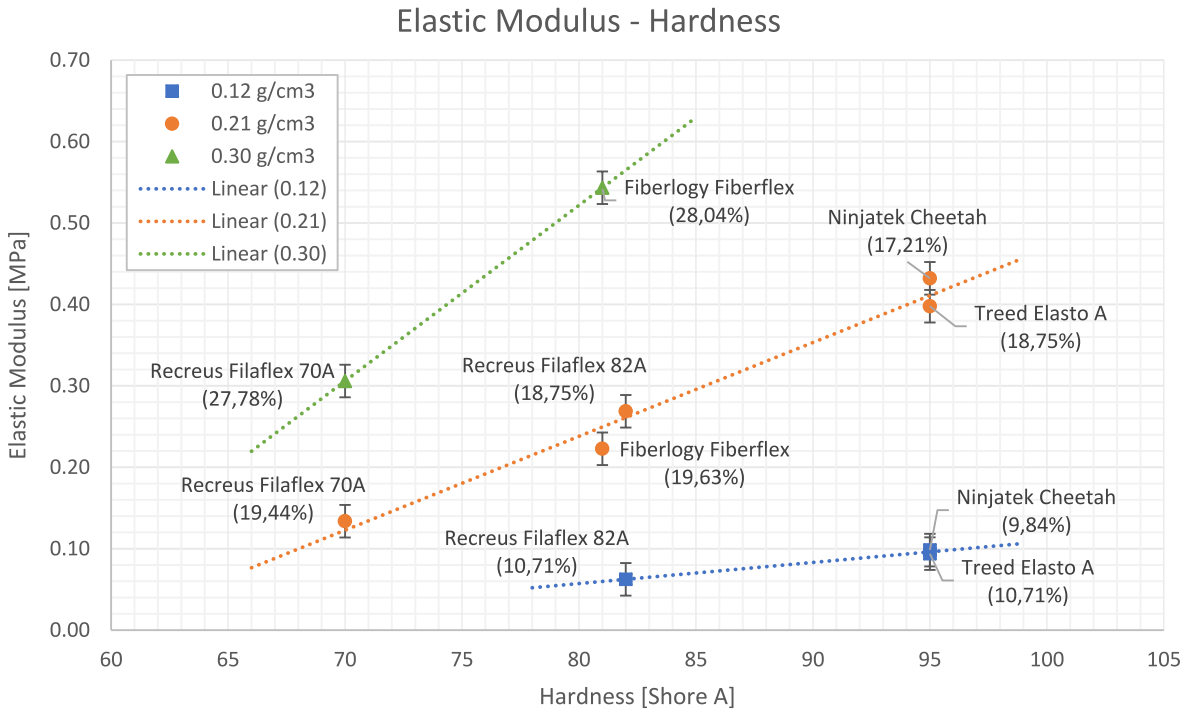

Fig. 11. Scatter plot that correlates the elastic modulus with the hardness on specimens made with 3D printing.

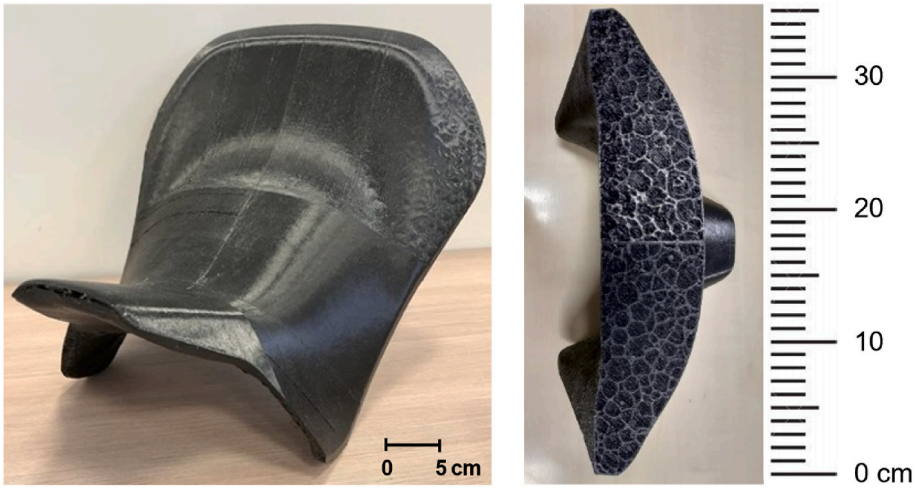

Fig. 12. First saddle prototype based on naked motorcycles with the detail of the inner section (right).

corresponding to different specimen densities, with the slope increasing as density rises. This graph serves as an experimental map describing the specimens' behaviour based on the three analysed parameters. By following the iso-lines, which represent constant density, one can determine either the filament hardness or the elastic modulus depending on specific requirements. This methodology opens substantial possibilities for foam prototyping across various applications, as the graph enables precise replication of desired behaviours. Through the analysis of force-displacement curves, it becomes possible to select the most appropriate curve according to the desired characteristics of the initial non-linear region and the slope of the linear region. The map in Fig. 11 provides all the necessary information to design foam with intermediate characteristics within the scatter plot. The map is generated based on experimental tests, which inherently include a certain degree of error. Data on density and Shore hardness are sourced from supplier datasheets, which, while not explicitly specifying measurement errors, are obtained following standardised procedures. Specifically, density measurements comply with ISO 1183, ASTM D792, which define the methodologies for determining the density of polymeric materials. Similarly, Shore hardness values are determined according to ISO 868, ASTM D2240, and ISO 7619, which establish the testing conditions and indenter types for accurate hardness assessment. These standards ensure the reliability and comparability of the reported material properties within the context of this study. The measurement errors observed across all tests were found to be below 0.02 MPa, as illustrated in Fig. 11. For the sake of clarity and readability, error intervals were not included in the earlier graphs. To expand this map further by including additional densities and material hardnesses, a 3D printer equipped with a pellet extruder would be advantageous, as it eliminates the limitations imposed by filament-based processes.

Economic considerations must always be factored in, as they are often decisive in selecting the appropriate manufacturing process. Additive manufacturing is particularly cost-effective for producing custom items or small batches, as its lower productivity compared to traditional methods is offset by its high flexibility. However, the production of foams as described earlier is unlikely to replace mass production due to the extended time and higher costs involved. For initial prototype development, such as for verifying design, functionality, and comfort, it proves highly advantageous, as it eliminates the need for mould production, reducing costs by an order of magnitude.

The stochastic infill, which mimics the closed-cell structure of foam created with blowing agents, has demonstrated effectiveness in producing components for impact absorption, customised padding, and flexible parts in rapid prototyping. This is merely the first step in the development of flexible parts with precisely controlled material responses. Future studies could investigate other aspects of these structures, such as the effect of external walls on stiffness. Currently, the specimens were not tested for compression in the X and Y directions due to the lack of uniform contact surfaces, resulting from the absence of external walls. For future tests in these directions, it will be essential to prevent delamination between layers.

Further exploration could involve newly introduced filaments containing blowing agents that generate microbubbles as they pass through the nozzle, altering the stiffness of the extruded material. These filaments demonstrate variable hardness depending on the extrusion temperature, offering enhanced flexibility during the manufacturing process and enabling the use of a single material across a wide range of applications. However, this introduces an additional variable that must be carefully managed to ensure consistent and high-quality outcomes. Additionally, the study could be enriched by analysing the fatigue behaviour of these structures to determine the number of cycles they can endure. Investigating the energy absorption characteristics, including hysteresis, would provide further insights into their performance and potential.

5. Conclusion

This research has successfully demonstrated the feasibility of producing polymeric foam models using additive manufacturing, specifically employing Material Extrusion (MEX) technology. The experimental findings confirm that specimens with stochastic infill patterns, mimicking the closed-cell structures of foams generated through blowing agents, can effectively achieve desired mechanical properties. Critical to tailoring the foam characteristics observed in the force-displacement graph are the density of the component (determined by infill percentage) and the hardness of the material used.

The study underscored the significance of material hardness during the initial deformation phase, where softer materials are advantageous for achieving low force under increasing deformation. Conversely, foam density primarily influences the slope of the linear region of the deformation curve, with adjustments to infill percentage playing a key role. Additionally, the foams produced in this study are characterized by solid top and bottom layers, without external walls, which significantly impact stiffness and alter the force-displacement response. Incorporating external walls in prototypes modifies these properties, highlighting their importance in designing foam components. The experimental map generated in this research, featuring iso-lines that indicate constant density, serves as a valuable design tool for creating foams with precisely tailored behaviours. It enables the selection of the most suitable filament hardness or elastic modulus according to

application-specific requirements. Further refinement of this map, incorporating additional densities and material hardnesses, could enhance the design process. Employing a 3D printer equipped with a pellet extruder would further optimize this approach by eliminating the constraints of filament-based systems.

This study establishes a robust foundation for the informed design of flexible parts with specific performance requirements, leveraging the experimental map to correlate behaviour with infill percentage and filament hardness. Producing components in the early stages of product development proves highly cost-effective, as it allows for the rapid creation of multiple models without the need to remake or modify traditional moulds for foam production (Fig. 12). Future research should explore the impact of incorporating external walls, providing a means to further control the properties of printed components. Additionally, investigating the use of filaments with variable Shore hardness could offer greater design flexibility and expand the range of applications.

CRediT authorship contribution statement

Andrea Montalti: Writing – review & editing, Writing – original draft, Supervision, Investigation, Data curation. **Patrich Ferretti:** Methodology, Funding acquisition, Data curation, Conceptualization. **Fiammetta Spano:** Writing – original draft, Methodology, Investigation, Formal analysis, Data curation. **Alfredo Liverani:** Supervision, Project administration.

Funding

This research did not receive any specific grant from funding agencies in the public, commercial, or not-for-profit sectors.

Declaration of Competing interest

The authors declare that they have no known competing financial interests or personal relationships that could have appeared to influence the work reported in this paper.

Acknowledgments

We would like to express our sincere thanks to Dr. Brugo for his invaluable contribution and crucial support in conducting the compression tests in the laboratory, which made the realization of this study possible. His expertise, dedication, and professionalism provided essential guidance throughout the experimental phases, significantly contributing to the quality and precision of the obtained results.

Data availability

Data will be made available upon reasonable request.

References

Aghvami-Panah, M., Azami, M., Kalia, K., Ameli, A., 2024. In situ foam 3D printed microcellular multifunctional nanocomposites of thermoplastic polyurethane and carbon nanotube. Carbon N Y 230, 119619. https://doi.org/10.1016/j.carbon.2024.119619.

Alessandri, G., et al., 2022. Virtual surgical planning, 3D-printing and customized bone allograft for acute correction of severe genu varum in children. J. Personalized Med. 12 (12), 2051. https://doi.org/10.3390/jpm12122051.

Anand Sankar, M., Deepak Lawrence, K., Mathew, J., 2023. Part Quality improvement of fused filament fabrication-based additive manufacturing by means of slicing software modifications. In: Lecture Notes in Mechanical Engineering. https://doi.org/10.1007/978-981-19-7612-4_21.

Bacciaglia, A., Ceruti, A., Liverani, A., 2022. Structural analysis of voxel-based lattices using 1D approach. 3D Print. Addit. Manuf. 9 (5). https://doi.org/10.1089/3dp.2020.0178.

Beloshenko, V., et al., 2021. Mechanical properties of flexible tpu-based 3d printed lattice structures: role of lattice cut direction and architecture. Polymers 13 (17). https://doi.org/10.3390/polym13172986.

Chen, Y., Das, R., Battley, M., 2017. Effects of cell size and cell wall thickness variations on the strength of closed-cell foams. Int. J. Eng. Sci. 120. https://doi.org/10.1016/j.ijengsci.2017.08.006.

Chisena, R.S., Shih, A.J., 2019. Analytical characterization and experimental validation of the material extrusion wave infill for thin-walled structures. Journal of Manufacturing Science and Engineering, Transactions of the ASME 141 (12). https://doi.org/10.1115/1.4045058.

Chu, C., Graf, G., Rosen, D.W., 2008. Design for additive manufacturing of cellular structures. Comput Aided Des Appl 5 (5). https://doi.org/10.3722/cadaps.2008.686-696.

Doshi, M., Mahale, A., Singh, S.K., Deshmukh, S., 2021. Printing parameters and materials affecting mechanical properties of FDM-3D printed Parts: perspective and prospects. In: Materials Today: Proceedings. https://doi.org/10.1016/j.matpr.2021.10.003.

Eida Nadirah, R., Badrulhisyam, A.J., Nurhayati, M.N., Rifqi Irzuan, A.J., Mohamad Asmidzam, A., Nor Syazwani, A.A., 2020. Preliminary study on the ergonomic design of motorcycle seat for comfort usage. Malaysian Journal of Public Health Medicine 20 (Specialissue1). https://doi.org/10.37268/MJPHM/VOL.20/NO.SPECIAL1/ART.700.

Emery, B., Revier, D., 2022. Applied viscous thread instability for manufacturing 3D printed foams. In: Proceedings - SCF 2022 - 7th Annual ACM Symposium on Computational Fabrication. https://doi.org/10.1145/3559400.3565596.

Esposito, C., Tammaro, D., Posabella, P., Villone, M.M., D'Avino, G., Maffettone, P.L., 2024. Orientation-Graded morphologies in microcellular foams through additive manufacturing. Ind. Eng. Chem. Res. 63 (42), 17949–17960. https://doi.org/10.1021/acs.iecr.4c02307.

Feng, Y.H., et al., 2019. Prediction of motorcycle seat styling based on grey modelling (1,1). Comput Aided Des Appl 16 (5). https://doi.org/10.14733/cadaps.2019.789-802.

Forés-Garriga, A., Pérez, M.A., Gómez-Gras, G., Reyes-Pozo, G., 2020. Role of infill parameters on the mechanical performance and weight reduction of PEI Ultem processed by FFF. Mater. Des. 193. https://doi.org/10.1016/j.matdes.2020.108810.

Gama, N.V., Ferreira, A., Barros-Timmons, A., 2018. Polyurethane Foams: Past, Present, and Future. https://doi.org/10.3390/ma11101841.

Gong, L., Kyriakides, S., Jang, W.Y., 2005. Compressive response of open-cell foams. Part I: morphology and elastic properties. Int. J. Solid Struct. 42 (5–6). https://doi.org/10.1016/j.ijsolstr.2004.07.023.

H S, B., Bonthu, D., Prabhakar, P., Doddamani, M., 2020. Three-dimensional printed lightweight composite foams. ACS Omega 5 (35). https://doi.org/10.1021/acsomega.0c03174.

Hassanien, M., Alkhader, M., Abu-Nabah, B.A., Abuzaid, W., 2023. A low-cost process for fabricating reinforced 3D printing thermoplastic filaments. Polymers 15 (2). https://doi.org/10.3390/polym15020315.

Kabir, M.E., Saha, M.C., Jeelani, S., 2006. Tensile and fracture behavior of polymer foams. Materials Science and Engineering: A 429 (1–2). https://doi.org/10.1016/j.msea.2006.05.133.

Kalia, K., Francoeur, B., Amirkhizi, A., Ameli, A., 2022. In situ foam 3D printing of microcellular structures using material extrusion additive manufacturing. ACS Appl. Mater. Interfaces 14 (19). https://doi.org/10.1021/ACSAMI.2C03014.

Kechagias, J.D., 2024. Surface roughness assessment of ABS and PLA filament 3D printing parts: structural parameters experimentation and semi-empirical modelling. Int. J. Adv. Des. Manuf. Technol. 134 (3–4), 1935–1946. https://doi.org/10.1007/s00170-024-14232-0.

Kristiawan, R.B., Imaduddin, F., Ariawan, D., Ubaidillah, Arifin, Z., 2021. "A review on the fused deposition modeling (FDM) 3D printing: filament processing. materials, and printing parameters," https://doi.org/10.1515/eng-2021-0063.

Liu, T., Burger, C., Chu, B., 2003. Nanofabrication in Polymer Matrices. https://doi.org/10.1016/S0079-6700(02)00077-1.

Llewelyn, G., Rees, A., Griffiths, C., Jacobi, M., 2020. A design of experiment approach for surface roughness comparisons of foam injection-moulding methods. Materials 13 (10). https://doi.org/10.3390/ma13102358.

Maiti, A., et al., 2016. 3D printed cellular solid outperforms traditional stochastic foam in long-term mechanical response. Sci. Rep. 6. https://doi.org/10.1038/srep24871.

Nian, Y., et al., 2024. Nature-inspired 3D printing-based double-graded aerospace negative Poisson's ratio metastructure: design, Fabrication, Investigation, optimization. Compos. Struct. 348, 118482. https://doi.org/10.1016/j.compstruct.2024.118482.

Panda, B., Leite, M., Biswal, B.B., Niu, X., Garg, A., 2018. Experimental and numerical modelling of mechanical properties of 3D printed honeycomb structures. Measurement 116. https://doi.org/10.1016/j.measurement.2017.11.037.

Papadopoulos, A.M., 2005. State of the art in thermal insulation materials and aims for future developments. Energy Build. 37 (1). https://doi.org/10.1016/j.enbuild.2004.05.006.

Parry, G.R., Felton, H.J., Ballantyne, R., Su, S., Hicks, B., 2023. Reducing prototype fabrication time through enhanced material extrusion process capability. In: Proceedings of the Design Society. https://doi.org/10.1017/pds.2023.303.

Pawar, A., Ausias, G., Corre, Y.M., Grohens, Y., Férec, J., 2022. Mastering the density of 3D printed thermoplastic elastomer foam structures with controlled temperature. Addit. Manuf. 58. https://doi.org/10.1016/j.addma.2022.103066.

Peng, B., Yang, Y., Ju, T., Cavicchi, K.A., 2021. "Fused filament fabrication 4D printing of a highly extensible, self-healing. Shape Memory Elastomer Based on Thermoplastic Polymer Blends,". https://doi.org/10.1021/acsami.0c18618.

Peng, K., et al., 2024. Microporous polylactic acid/chitin nanocrystals composite scaffolds using in-situ foaming 3D printing for bone tissue engineering. Int. J. Biol. Macromol. 279, 135055. https://doi.org/10.1016/j.ijbiomac.2024.135055.

Pontiff, T., 2014. Foaming agents for foam extrusion. In: Foam Extrusion: Principles and Practice, second ed. https://doi.org/10.1201/b16784

Rodríguez-Parada, L., De La Rosa, S., Mayuet, P.F., 2021. Influence of 3D-printed TPU properties for the design of elastic products. Polymers 13 (15). https://doi.org/10.3390/polym13152519.

Salifu, S., Desai, D., Ogunbiyi, O., Mwale, K., 2022. Recent Development in the Additive Manufacturing of Polymer-Based Composites for Automotive Structures—A Review. https://doi.org/10.1007/s00170-021-08569-z.

Seng, C.T., A/l Eh Noum, S.Y., A/l Sivanesan, S.K., Yu, L.J., 2020. Reduction of hygroscopicity of PLA filament for 3D printing by introducing nano silica as filler. AIP Conf. Proc. https://doi.org/10.1063/5.0001927.

Shin, E.J., Park, Y., Jung, Y.S., Choi, H.Y., Lee, S., 2022. Fabrication and characteristics of flexible thermoplastic polyurethane filament for fused deposition modeling three-dimensional printing. Polym. Eng. Sci. 62 (9). https://doi.org/10.1002/pen.26075.

Ugadi, S., Muduli, B., Yeshamoni, S., Mukherjee, M., Neelakantan, L., 2024. Electroless copper plating of 3D-printed polymer foam: a promising method to fabricate electrodes for denitrification. Mater. Lett. 372, 137019. https://doi.org/10.1016/j.matlet.2024.137019.

Viscardi, M., Arena, M., Siano, D., 2016. Design and testing of a prototype foam for lightweight technological applications. International Journal of Mechanics 10.

Xu, N., Qian, Y., Yu, J., Leung, C.K.Y., 2022. Tensile performance of 3D-printed Strain-Hardening Cementitious Composites (SHCC) considering material parameters, nozzle size and printing pattern. Cem. Concr. Compos. 132. https://doi.org/10.1016/j.cemconcomp.2022.104601.

Yi, L., et al., 2023. A new gradient infill design method for material extrusion using density-based topology optimization and G-code extension. Manuf Lett 37, 21–25. https://doi.org/10.1016/j.mfglet.2023.06.003.

Zhou, M., Chen, B., Li, Y., Jiang, J., Zhai, W., 2023. Enhanced interfacial adhesion and increased isotropy of 3D printed parts with microcellular structure fabricated via a micro-extrusion CO2-foaming process. Adv. Eng. Mater. 25 (8). https://doi.org/10.1002/adem.202201468.